doi:10.14311/ppt.2025.3.233
Plasma Physics and Technology **12**(3):233–238, 2025

THE IMPACT OF OXYGEN CONTENT ON THE ABLATION MECHANISM OF GASSING MATERIALS UNDER ARC ACTION

Qian Wang[a,*], Yi Shang[a], Weidong Cao[b], Wanmeng Zhao[a], Yuxuan Liu[a], Xu Zhong[a]

[a] *School of Science, Xi'an University of Technology, Xi'an, Shaanxi, China*

[b] *College of Electrical Engineering, Xi'an Jiaotong University, Xi'an, Shaanxi, China*

[*] qianwang@xaut.edu.cn

Abstract. With the rapid development of Renewable energy, DC power system, Energy Storage System and Rail Transit etc, the demand of high performance Direct Current circuit breakers is increasing significantly. Gassing materials can improve the interruption capability during the arc ignition process, however, the decomposition process and reaction products will be affected by the onsite environment, such as pressure, oxygen concentration and humidity. Using molecular dynamics simulations, the decomposition process of PA66 under an electric field at varying oxygen contents was analyzed. The results show that the introduction of oxygen accelerates the decomposition of PA66, not only promoting hydrogen generation but also suppressing the formation of tar and coke, and provides a preliminary standard for choosing the qualified gassing materials.

Keywords: Breaker, Decomposition, PA66, ReaxFF, Oxygen Content.

1. Introduction

To support Chinese carbon-peaking and carbon-neutrality goals, green energies such as photovoltaics and hydrogen are expanding rapidly [1, 2]. In power transmission and distribution networks, DC circuit breakers play a decisive role: when faults like short-circuits or overloads occur, the breaker opens to prevent greater damage. Unlike their AC counterparts, DC breakers lack a natural current-zero crossing, making arc extinction far more difficult. The resulting arcs can erode contacts and even trigger equipment failure or fire. Special arc-quenching technologies are therefore essential to cool the arc.

Gassing materials are purpose-designed for this task. During interruption, the intense arc decomposes the material, rapidly releasing large volumes of thermally conductive gases (e.g., hydrogen) that cool the arc, constrict its column, and restore dielectric strength-thereby improving breaking capacity and overall breaker performance [3]. Yet, real operating environments vary. A breaker may be exposed to atmospheres with different oxygen levels, from low-oxygen sealed chambers to ambient air during maintenance. Oxygen significantly alters the pyrolysis of PA66, changing both the composition and yield of its decomposition products. Investigating how oxygen content affects PA66 pyrolysis will therefore provide the theoretical basis for optimizing gassing material formulations and breaker designs, ensuring reliable operation under diverse conditions and enhancing the safety and stability of power systems.

To select optimal gassing materials, researchers have conducted extensive experimental and simulation studies. Yet the high cost of experiments and the limitations of conventional simulations call for more economical approaches. Reactive force field (ReaxFF) [4], a reactive molecular dynamics method, has emerged as a powerful alternative. Unlike traditional molecular dynamics, ReaxFF can track the real-time making and breaking of chemical bonds and can handle systems containing millions of atoms. In this work, ReaxFF is employed to investigate how oxygen content influences the pyrolysis of gassing materials and the characteristics of their decomposition products. A deeper understanding of oxygen's effect on PA66 pyrolysis will provide theoretical guidance for optimizing gassing material formulations and selecting circuit breakers, thereby enhancing the safety and stability of power systems.

2. Model Construction and Parameter Settings

ReaxFF enhances the force field of classical molecular dynamics by incorporating the concepts of bond order and bond energy. It determines the formation or breaking of bonds between atoms based on their interatomic distances. Additionally, ReaxFF introduces the effects of van der Waals forces and Coulomb forces, building upon the principles of Newtonian mechanics. Formula (1.1) presents the commonly used energy composition formula for the ReaxFF system, which was proposed by K. Chenoweth. For details on the meaning of each parameter, please refer to reference [5].

First, monomeric PA66 and O_2 molecules were modeled in Materials Studio. Figure 1 shows the corresponding workflow. For the simulation, we selected a PA66 chain with a polymerization degree of 8 and

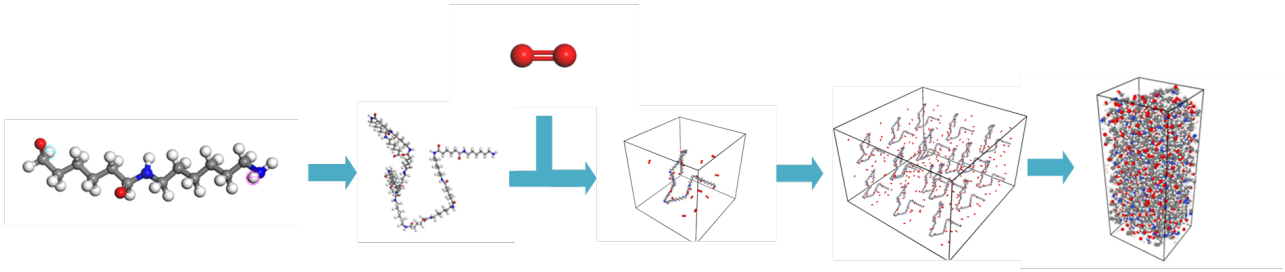

Figure 1. Model establishment flow chart.

placed water molecules within a $5\times5\times5\,nm^3$ box, balancing computational efficiency with accuracy. PA66 molecules and their polymer chains are depicted in Figure 1, where different colors indicate different types of PA66 atoms. All molecular dynamics simulations were conducted using the Large-scale Atomic-Molecular Massively Parallel Simulator (LAMMPS).

$$\begin{aligned} E_{\text{system}} =& E_{\text{bond}} + E_{\text{lp}} + E_{\text{over}} + E_{\text{under}} + E_{\text{val}} + \\ & E_{\text{pen}} + E_{\text{coa}} + E_{\text{C2}} + E_{\text{triple}} + E_{\text{tors}} + \\ & E_{\text{conj}} + E_{\text{H-bond}} + E_{\text{vdWaals}} + \\ & E_{\text{Coulomb}} \end{aligned} \quad (1)$$

In Reference [6], a simulation method was proposed to mimic the heating effect of arc radiation by applying a periodic electric field to the system. In this method, the frequency and intensity of the applied electric field are two values that need to be determined. According to the method described in the paper, we determined the electric field frequency to be $3653\,cm^{-1}$; the initial electric field strength E_0 was set at $0.3\,V/Å$. Once the system temperature reached the set temperature, the electric field strength was then adjusted to $10^{-5}\,V/Å$ to simulate the shielding effect of the ablation products. This adjustment is necessary because if the electric field strength is too low, the temperature increase will be insignificant, significantly prolonging the simulation time; conversely, if the electric field strength is too high, the temperature will rise too rapidly, potentially leading to unrealistic molecular configurations.

3. Decomposition of PA66 under Various Oxygen Contents

3.1. Effect on decomposition rate of PA66

Figure 2 shows the PA66 population as a function of time. In the absence of oxygen (0 % O_2), PA66 decomposes most slowly, with complete decomposition not reached until 53 ps. As the oxygen content rises, both the decomposition rate and the onset of degradation accelerate. This trend is attributed to the polar amide groups (-CONH-) along the PA66 backbone and the reactive carboxyl (-COOH) and amino ($-NH_2$) termini. At the given temperature, oxygen readily participates in oxidation reactions at these polar sites, promoting chain scission and re-combination. These structural

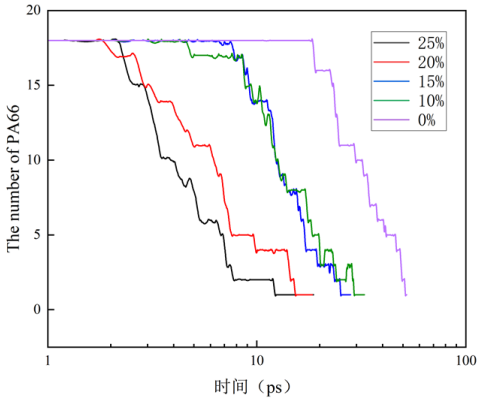

Figure 2. Variation in the Number of PA66 Molecules.

changes lower the thermal stability of PA66, rendering it more susceptible to pyrolysis.

Figure 3 illustrates the reaction pathway of an O_2 molecule. It is observed that, upon entering the reaction, the O=O double bond first converts into a single bond, giving each oxygen atom a radical character. One of these oxygen radicals then combines with a free hydrogen atom, while the other attaches to a $\cdot CH_2$ radical; subsequently, the O–O bond breaks completely. Because a trajectory frame is extracted every 5000 steps, the final frame shown in Figure 3 already captures a further reaction product.

Table 1 lists the major products obtained from five systems with different oxygen contents. The dominant products are H_2, CO and H_2O. With increasing oxygen content, the yield of CO_2 gradually rises, while those of CH_4 and C_2H_6 steadily decline. Thus, the primary pyrolysis products of PA66 shift from hydrocarbons such as CH_4 and C_2H_6 to smaller oxygen-containing molecules like CNH and CO_2. This trend arises because the proportion of oxidation reactions increases at higher oxygen levels, allowing intermediates to react more completely.

3.2. Effect on the quantities of reaction products

Figure 4 shows the evolution curves of H_2 quantity. It can be observed that, in every system, the amount of H_2 increases monotonically with time. As the oxygen content rises (from the purple to the black curve),

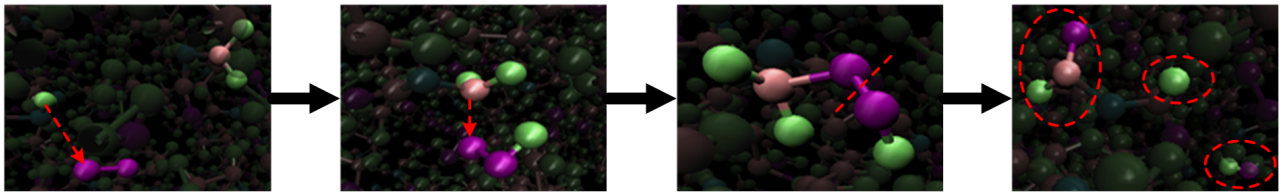

Figure 3. Reaction process involving an oxygen molecule (purple atoms denote oxygen, green hydrogen, and brown carbon).

Products	25%O_2	20%O_2	15%O_2	10%O_2	0%O_2
H_2	888	803	673	584	432
H_2O	306	309	341	283	124
CO	393	302	152	108	76
CO_2	27	22	16	11	2
CH_4	1	13	20	30	20
CNH	15	10	5	11	5
C_2H_6	1	1	2	3	13

Table 1. Main Products.

the onset of decomposition occurs earlier, the rate of decomposition accelerates, and the ultimate yield of H_2 grows correspondingly. This is because higher oxygen content causes more chemical bonds in the PA66 chains to rupture, producing a larger number of free radicals. These radicals subsequently recombine to form H_2, thereby increasing its yield. Moreover, from the perspective of reaction type, the reactions involving O_2 are oxidative and exothermic; the heat released excites more functional groups into reactive states, accelerating the scission and rearrangement of PA66 chains and thus further promoting hydrogen generation.

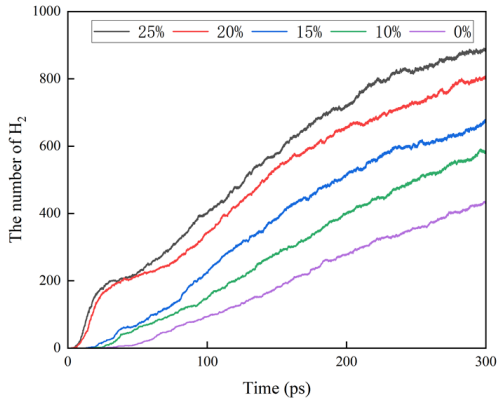

Figure 4. Variation in the Quantity of Hydrogen Gas.

Figure 5 depicts the formation pathway of a specific hydrogen molecule. As shown, the two hydrogen atoms in the H_2 originate separately from the intermediates H_2O and NH_2, each donating one H atom to form the H_2 molecule. The oxygen in H_2O and the nitrogen in NH_2, in turn, come from the initial O_2 molecule and the nitrogen originally present in PA66, respectively; both H_2O and NH_2 are produced through a series of complex reactions.

3.3. The Impact on Tar and Coke

During the interruption process of a circuit breaker, carbonaceous residues progressively deposit on the material surface as the number of interruptions increases. These deposits hinder subsequent gas generation and weaken the arc-quenching and cooling effects, making the study of carbonaceous residues crucial. Such residues are typically classified according to the number of carbon atoms in a single molecule: C1–C4 are gaseous hydrocarbons, C5–C12 are light tars, and C13–C40 and C40+ are heavy tars and coke.

Figure 6 presents the evolution of the quantities of the four carbon-chain classes. Panels (a)–(d) correspond, respectively, to C1–C4, C5–C12, C13–C40, and C40+. Initially, because the PA66 molecule contains 96 carbon atoms, the population of C40+ molecules decreases continuously, while the other three classes rise rapidly. Once all PA66 molecules have decomposed, the counts of C1–C4 and C5–C12 reach maxima and that of C40+ attains its minimum. Subsequently, the large number of small molecules makes intermolecular collisions more frequent; polymerization and condensation reactions between these small chains lead to the formation of larger molecules, causing the quantities of C1–C4 and C5–C12 to decline gradually.

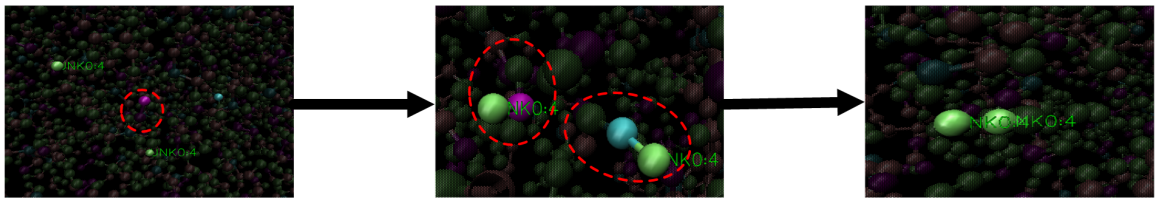

Figure 5. Origin and formation pathway of a specific hydrogen molecule (purple: oxygen, green: hydrogen, blue: nitrogen).

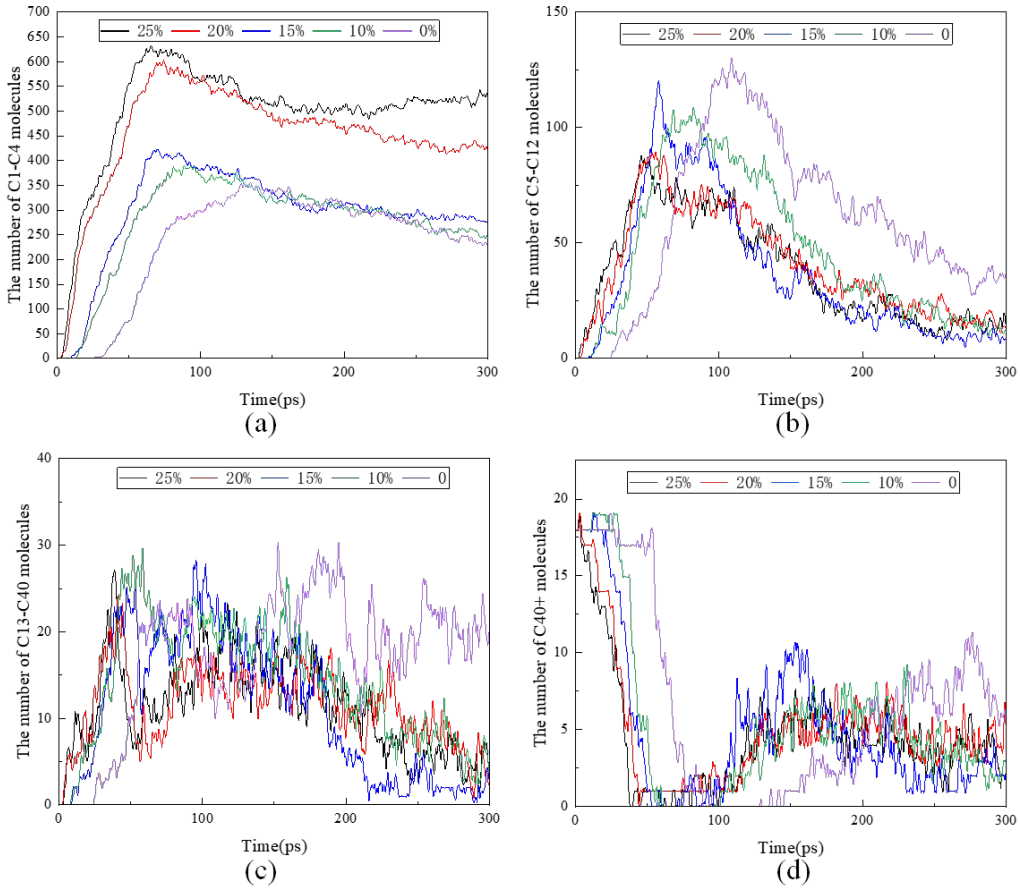

Figure 6. Variation in the number of different carbon-chain species(a: C1–C4 molecules; b: C5–C12 molecules; c: C13–C40 molecules; d: C40+ molecules).

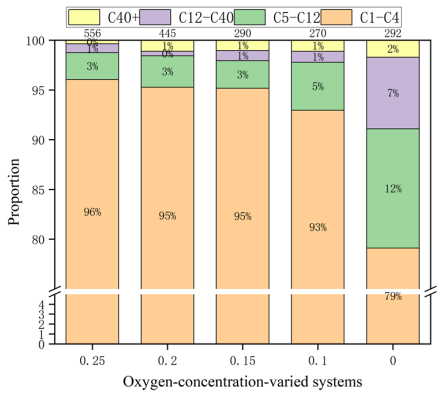

Figure 7. Proportions of Different Types of Carbon Chains Under Various Oxygen Concentrations.

Furthermore, under oxygen-containing conditions the populations of C5–C12, C13–C40, and C40+ are consistently lower than those under oxygen-free conditions, whereas the count of C1–C4 is higher. This indicates that increasing oxygen content promotes the formation of small C1–C4 molecules while suppressing the production of tar and coke.

As shown in Figure 7, which presents the proportions of various carbon-chain species under different oxygen concentrations, the fraction of C1–C4 small molecules rises steadily with increasing oxygen content, whereas the proportion of larger C5+ molecules correspondingly declines. This further confirms that oxygen promotes the conversion of macromolecules into smaller fragments while inhibiting the formation of tar and coke. Consequently, it is reasonable to

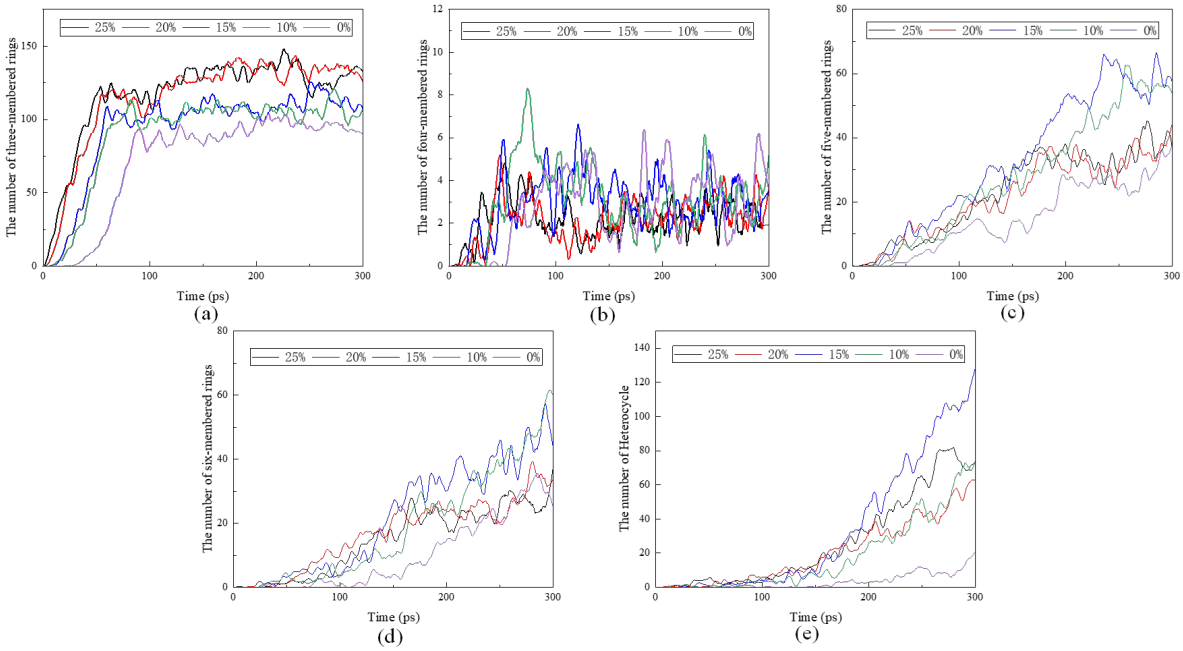

Figure 8. Variation in the quantities of different carbon-ring types.

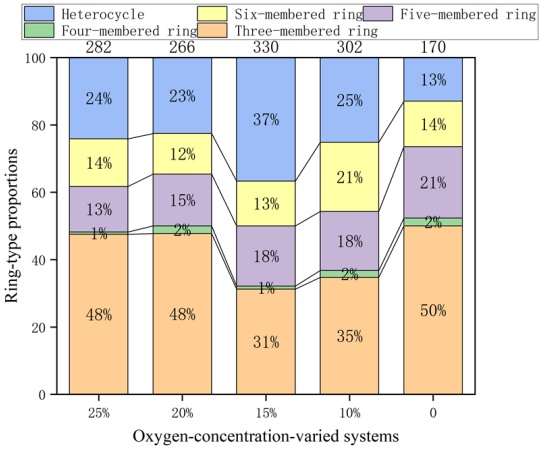

Figure 9. Proportions of various ring types under different oxygen concentrations.

conclude that higher oxygen levels will reduce coke deposition within the circuit breaker, accelerate arc extinction, and enhance the device's interrupting performance.

Because tar and coke consist primarily of carbon rings, the molecular structure and pyrolysis pathways of different polyamide materials directly influence the product distribution. Therefore, a comparative analysis of the types and quantities of carbon rings formed from different gassing materials is essential. Figure 8 compares the evolution curves of various carbon rings under oxygen-free and normal-oxygen conditions. Over time, the number of three-membered rings peaks before 100 ps and then stabilizes; the higher the oxygen concentration, the larger the final population of three-membered rings. Four-membered rings remain scarce and essentially constant owing to their inherent instability. The counts of all other ring types rise continuously with time, yet increase in oxygen content progressively reduce these larger rings. This trend arises because, under low-oxygen conditions, pyrolysis favors the formation of multi-ring structures: oxidation is limited, so hydrocarbons are converted mainly via pyrolytic rather than oxidative routes into liquid or gaseous products. As oxygen content increases, oxidation becomes dominant, converting more hydrocarbons into CO_2 and H_2O and consequently lowering the yield of multi-ring species. Moreover, elevated oxygen levels promote further oxidation and fragmentation of multi-ring intermediates, diminishing the final abundance of cyclic structures.

Figure 9 shows the proportion of each ring type under different oxygen concentrations. Overall, three-membered rings account for the highest share. As the oxygen concentration increases, the fraction of three-membered rings first drops from 50 % in the oxygen-free system to 31 % at 15 % O_2, while the proportion of heterocycles rises from 13 % to 37 %. When the oxygen concentration is raised further, the trend reverses: the three-membered ring content increases again, and the heterocycle content declines. This behavior can be explained as follows. At low oxygen levels, the limited oxygen preferentially attacks the highly strained three-membered rings (C_3) and side chains, opening them to yield carboxylic acids, aldehydes, and other small molecules; consequently, the three-membered ring fraction falls from 50 % to 31 %. Simultaneously, N/O-containing fragments undergo dehydrogenation-condensation reactions to form heterocycles such as pyridines and benzofurans, so the

heterocycle proportion increases from 13 % to 37 %. At higher oxygen concentrations, the elevated concentration of oxygen radicals leads to deeper oxidation of both heterocycles and larger aromatic rings, cleaving C–N and C–O bonds and causing the heterocycle fraction to decrease. Surplus oxygen radicals, however, can "back-bite" olefinic or alkyl radicals to generate new three-membered-ring transition states; the associated exothermicity accelerates cyclization, driving the three-membered ring content back up.

4. Conclusion

In summary, we can draw the conclusion that the introduction of oxygen accelerates the decomposition of PA66, not only promoting the generation of hydrogen gas but also inhibiting the formation of tar and coke. Therefore, it can be reasonably inferred that the addition of high oxygen content will reduce the formation of coke in circuit breakers, accelerate arc extinction, and enhance the interrupting performance of the circuit breakers.

Acknowledgements

Qian Wang was supported by the National Natural Science Foundation of China (52277163) and Shaanxi Provincial Department of Education key laboratory project (2022JS025).

References

[1] W. Chenyang, D. Qianqian, Z. Kai, et al. A hybrid model for photovoltaic power prediction of both convolutional and long short-term memory neural networks optimized by genetic algorithm. *Acta Phys. Sin.*, 69(10):100701, 2020. doi:10.7498/aps.69.20191935.

[2] H. Liu, J. Dankwa Ampah, S. Afrane, et al. Potential benefits and trade-offs associated with hydrogen transition under diverse carbon dioxide removal strategies. *Science Bulletin*, 11 2023. doi:10.1016/j.scib.2023.10.033.

[3] W. Junliang and W. Ming-di. Optimization design and experimental study of mccb arc chamber. *Journal of Engineering Design*, 24(4):480–486, 2017. doi:10.3785/j.issn.1006-754X.2017.04.016.

[4] A. C. T. van Duin, S. Dasgupta, F. Lorant, and W. A. Goddard. Reaxff: a reactive force field for hydrocarbons. *The Journal of Physical Chemistry A*, 105(41):9396–9409, 2001. doi:10.1021/jp004368u.

[5] M. Kowalik, C. Ashraf, B. Damirchi, et al. Atomistic scale analysis of the carbonization process for C/H/O/N-based polymers with the reaxff reactive force field. *The Journal of Physical Chemistry B*, 123(25):5357–5367, 2019. doi:10.1021/acs.jpcb.9b04298.

[6] W. Cao, X. Li, Y. Zhang, et al. Atomic-scale insight into arc plasma radiation-induced gassing materials ablation: photothermal decomposition behavior. *Journal of Physics D: Applied Physics*, 57(19):195204, feb 2024. doi:10.1088/1361-6463/ad2562.